Fast optimization algorithm on complex oblique manifold for hybrid precoding in millimeter wave MIMO systems

Hiroyuki Kasai*

June 30, 2018

Abstract

This paper considers a hybrid precoder design for millimeter wave (mmWave) systems. The conventional works suffer from performance loss in spectral efficiency, and also suffer from high complexities of optimization algorithms in terms of iteration as well as processing time. This paper proposes a new fast optimization algorithm in terms of iteration and processing time without rendering the decrease of spectral efficiency. Exhaustive evaluations demonstrate that the proposed algorithm with an improved calculation algorithm of the gradient and a single-loop iteration architecture yields comparable or faster processing speed than the state-of-the-art algorithms while keeping spectral efficiency near-optimal.

The codes of the proposed algorithm is implemented in the MATLAB toolbox Manopt [16] and are available at `https://github.com/hiroyuki-kasai/HybridPrecodingOpt`.

1 Introduction

A *millimeter wave* (mmWave) system, of which bounds ranges from 30 GHz to 300 GHz, provides high data rates over cellular networks [1, 2, 3, 4, 5]. The short wavelength of the mmWave system allows its transceivers to facilitate a large number of antenna arrays. The mmWave system leverages the multiple-input and multiple-output (MIMO) through such large antenna arrays to provide sufficient received signal power. However, the traditional MIMO systems deploy either fully analog beamforming at the radio frequency (RF) or fully digital precoding at the baseband circuits which control both phase shifts and amplitudes of incoming signals [6]. Subsequently, this makes it hard to devote itself to a separate RF chain[1] with its components for each antenna, resulting in high hardware costs and high power consumptions in large-scale MIMO systems [4, 3, 7, 8]. *Hybrid precoding(-beamforming)*, originally proposed in [9, 10], is the most promising approach to solve this problem, which combines *large*-dimensional *analog* precoding (or beamforming) via *phase shifters* with *lower*-dimensional *digital* baseband precoding. Hybrid precoding drastically reduces the number of RF chains from the number of antenna elements, which is needed in the fully digital scheme, into, at least, the number of data streams [11, 6].

The design of precoder and the decoder of the mmWave system is handled as two sub-problems, i.e., the precoding and decoding problems [11, 12, 13, 14]. The maximization of spectral efficiency approximately boils down to a minimization problem of the Euclidean distance between the *fully digital precoder* $\mathbf{F}_{\text{opt}}$ and the hybrid precoder, where $\mathbf{F}_{\text{opt}}$ is the unconstrained singular

*Graduate School of Informatics and Engineering, The University of Electro-Communications, Tokyo, Japan (`kasai@is.uec.ac.jp`).

[1]Up converter, down converter, digital-to-analog converter (DAC), analog-to-digital converter (ADC), mixers, and power amplifiers [6].

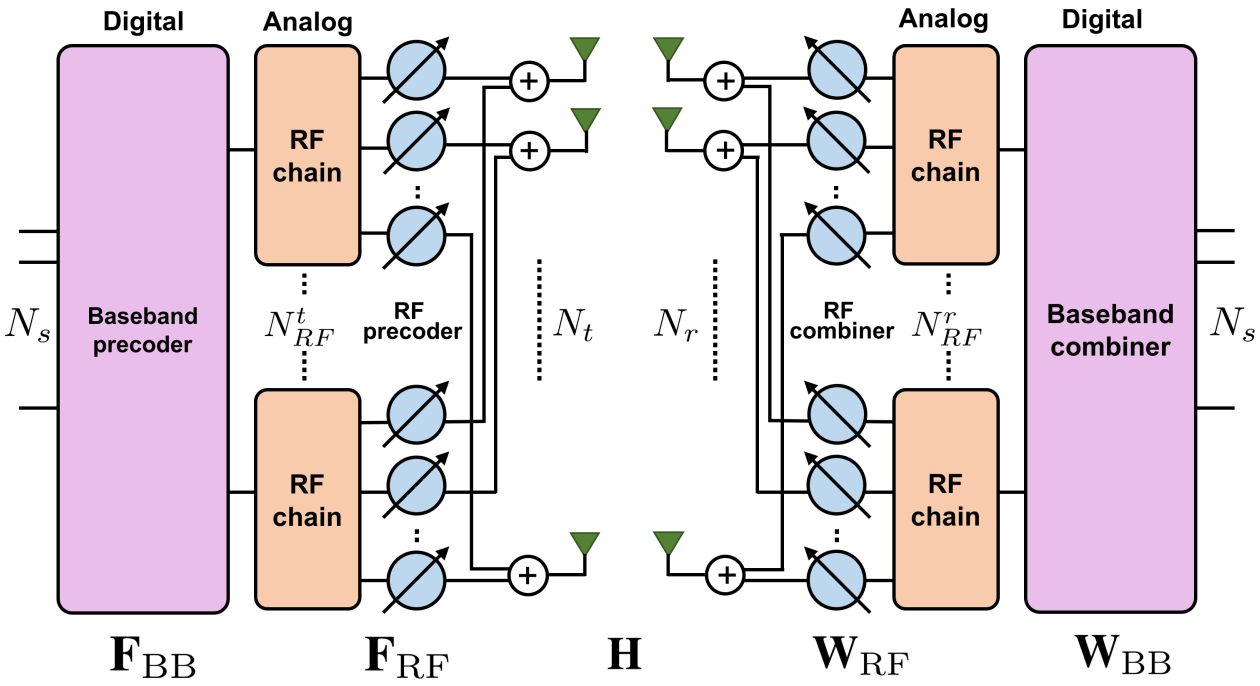

Figure 1: Hybrid precoder in mmWave MIMO system [11, 14].

value decomposition (SVD)-based precoding matrix. This problem is further formulated as a *matrix factorization* problem of $\mathbf{F}_{\mathrm{opt}}$ with a product of the digital *baseband precoder* matrix $\mathbf{F}_{\mathrm{BB}}$ and the analog *RF precoder* (or beamforming) matrix $\mathbf{F}_{\mathrm{RF}}$. The noteworthy point is that the phase shifters impose an additional *element-wise unit modulus* constraints on $\mathbf{F}_{\mathrm{RF}}$. For this particular problem, addressing the spatial structure of mmWave systems with large antenna arrays, Ayach et al. translated it into a *sparse reconstruction* problem, and solves it by the orthogonal matching pursuit (OMP) algorithm [11, 12]. However, this restriction on the space of feasible analog precoding solutions causes some decrease of spectral efficiency. Yu et al. proposed an alternative minimization algorithm, called MO-AltMin, based on a *manifold optimization* technique by embedding the unit modulus constituents on $\mathbf{F}_{\mathrm{RF}}$ into a product of multiple circles in the complex plane [14, Section III]. Although MO-AltMin provides near-optimal spectral efficiency, it suffers from not only slow down of the convergence speed of the procedure due to its *nested-loop* architecture between $\mathbf{F}_{\mathrm{BB}}$ and $\mathbf{F}_{\mathrm{RF}}$, but also an extremely high complexity to handle big matrices due to the Kronecker product. Therefore, Yu et al. proposed, in parallel, an alternative low-complexity algorithm, called PE-AltMin [14, Section IV]. It is, however, hindered by the decrease of spectral efficiency when the number of transmit chains increases, and also hindered by a high complexity originating in the SVD calculation per iteration for a big $\mathbf{F}_{\mathrm{opt}}^H\mathbf{F}_{\mathrm{RF}}$ matrix. Finally, Zanjani et al. proposed a gradient-based approach to maximize directly the mutual information instead of the approximated Euclidean distance problem, but it requires a high complexity [15].

This paper proposes a new fast optimization algorithm in terms of iteration and processing time without rendering the decrease of spectral efficiency. Following the same line of the strategy of MO-AltMin, the calculation algorithm of the gradient is modified to avoid big matrix calculations originating in the Kronecker product. Furthermore, a *single-loop* architecture of the alternating strategy between $\mathbf{F}_{\mathrm{BB}}$ and $\mathbf{F}_{\mathrm{RF}}$ is also proposed to alleviate the slow convergence produced by the

nested-loop architecture in MO-AltMin. These techniques allow the proposed algorithm to achieve comparable or faster processing speed than not only MO-AltMin but also PE-AltMin while keeping spectral efficiency higher than the state-of-the-art algorithms. The codes of the proposed algorithm is implemented in the MATLAB toolbox Manopt [16] and are available at `https://github.com/hiroyuki-kasai/HybridPrecodingOpt`.

2 Preliminaries

2.1 Notations

The scalars are represented with lower-case letters $(a, b, \ldots)$, vectors are with bold lower-case letters $(\boldsymbol{a}, \boldsymbol{b}, \ldots)$, and matrices are with bold-face capitals $(\mathbf{A}, \mathbf{B}, \ldots)$. $(\mathbf{A})_{i,j}$ represents the element of $\mathbf{A}$ at (i, j). $\mathbf{A}^T$. $\mathbf{A}^*$ and $\mathbf{A}^H$ are designated for the transpose, conjugate, and conjugate transpose of $\mathbf{A}$, respectively. The Moore-Penrose pseudo inverse of $\mathbf{A}$ is denoted as $\mathbf{A}^\dagger$. $\mathrm{vec}(\mathbf{A})$ and $\mathrm{vec}^{-1}(\mathbf{A})$ are vectorization and inverse-vectorization operators, respectively. $\mathbb{E}[\cdot]$ represents the expectation, and Real$[\cdot]$ extracts the real part of a complex variable. $\|\cdot\|_F$ denotes the Frobenius norm. $\otimes$ and $\circ$ denote the Kronecker and Hadamard products of two matrices.

2.2 System model

A single-user (point-to-point) multi-stream mmWave MIMO system is illustrated in Figure 1, in which a transmitter equipped with N_t antennas and N_{RF}^t RF chains and a receiver with N_r antennas and N_{RF}^r RF chains communicate via N_s data streams. N_s is constrained to be bounded as $N_s \leq N_{RF}^t \leq N_t$ and $N_s \leq N_{RF}^r \leq N_r$. This hardware architecture enables the transmitter to apply $N_{RF}^t \times N_s$ digital baseband precoder $\mathbf{F}_{\mathrm{BB}} \in \mathbb{R}^{N_{RF}^t \times N_s}$ using its N_{RF}^t transmit chains, followed by an $N_t \times N_{RF}^t$ analog RF precoder $\mathbf{F}_{\mathrm{RF}} \in \mathbb{R}^{N_t \times N_{RF}^t}$. Thus, the transmitted signal can be represented as $\boldsymbol{y} = \mathbf{F}_{\mathrm{RF}}\mathbf{F}_{\mathrm{BB}}\boldsymbol{s}$ $(\in \mathbb{R}^{N_t})$, where $\boldsymbol{s} \in \mathbb{R}^{N_s}$ is the the symbol vector with $\mathbb{E}[\boldsymbol{s}\boldsymbol{s}^H] = \frac{1}{N_s}\mathbf{I}_{N_s}$. For this system, The normalized transmit power constraint, i.e., $\|\mathbf{F}_{\mathrm{RF}}\mathbf{F}_{\mathrm{BB}}\|_F^2 = N_s$, is imposed. More importantly, the analog precoders are implemented with phase shifters to control the phases of the signals. Therefore, all the nonzero elements of $\mathbf{F}_{\mathrm{RF}}$ should satisfy the element-wise unit modulus constrains, i.e., $|(\mathbf{F}_{\mathrm{RF}})_{i,j}| = 1$.

3 Proposed optimization algorithm

This section defines the problem formulations, and then the proposed algorithm and its complexity are described in detail.

3.1 Problem formulation [11, 14]

The following problem (1) has been shown as an equivalent formulation to maximize spectral efficiency [11, 13, 14]. This can be intuitively understandable since the optimal hybrid precoders is suffciently close to the unconstrained optimal fully digital precoder. Here, because the optimal fully digital precoder matrix $\mathbf{F}_{\mathrm{opt}} \in \mathbb{R}^{N_t \times N_s}$ includes the eigen vectors of the channel matrix $\mathbf{H}$, $\mathbf{F}_{\mathrm{opt}}$ equivalently becomes the first N_s columns of $\mathbf{V}$, where $\mathbf{V}$ is derived from the SVD of the channel $\mathbf{H}$, i.e., $\mathbf{H} = \mathbf{U}\boldsymbol{\Sigma}\mathbf{V}^H$. Consequently, based on this $\mathbf{F}_{\mathrm{opt}}$, the problem is formulated as

$$\begin{aligned} \min_{\mathbf{F}_{\mathrm{RF}}, \mathbf{F}_{\mathrm{BB}}} \quad & \|\mathbf{F}_{\mathrm{opt}} - \mathbf{F}_{\mathrm{RF}}\mathbf{F}_{\mathrm{BB}}\|_F \\ \text{subject to} \quad & |(\mathbf{F}_{\mathrm{RF}})_{i,j}| = 1, \quad \|\mathbf{F}_{\mathrm{RF}}\mathbf{F}_{\mathrm{BB}}\|_F^2 = N_s. \end{aligned} \tag{1}$$

Furthermore, the extended problem formulation for multi-carrier techniques such as the OFDM system to alleviate the effect of the multi-path fading can be defined as

$$\begin{aligned} \min_{\mathbf{F}_{\mathrm{RF}},\mathbf{F}_{\mathrm{BB}}[l]} \quad & \sum_{l=1}^{L-1} \|\mathbf{F}_{\mathrm{opt}}[l] - \mathbf{F}_{\mathrm{RF}}\mathbf{F}_{\mathrm{BB}}[l]\|_F \\ \text{subject to} \quad & |(\mathbf{F}_{\mathrm{RF}})_{i,j}| = 1, \quad \|\mathbf{F}_{\mathrm{RF}}\mathbf{F}_{\mathrm{BB}}[l]\|_F^2 = N_s, \end{aligned} \tag{2}$$

where L is the total number of sub-carriers, and $l \in [0, L-1]$ is the sub-carrier index. $\mathbf{F}_{\mathrm{opt}}[l]$ and $\mathbf{F}_{\mathrm{BB}}[l]$ are the optimal digital precoder and the baseband precoder for the l-th sub-carrier, respectively.

3.2 Proposed algorithm

The narrowband mmWave system is first addressed for simplicity. Due to the element-wise unit modulus constrains on $\mathbf{F}_{\mathrm{RF}}$, i.e., $|(\mathbf{F}_{\mathrm{RF}})_{i,j}| = 1$, the vectorized representation of $\mathbf{F}_{\mathrm{RF}}$, i.e., $\mathrm{vec}(\mathbf{F}_{\mathrm{RF}}) \in \mathbb{R}^{N_t N_{RF}^t}$, forms a *complex oblique manifold* $\mathcal{OB}(m, \mathbb{C})$, where $\mathcal{OB}(m, \mathbb{C}) = \{\mathbf{X} = [\boldsymbol{x}_1, \cdots, \boldsymbol{x}_m] \in \mathbb{C}^{n \times m} : \|\boldsymbol{x}_1\| = \cdots = \|\boldsymbol{x}_m\| = 1\}$ with $m = N_t N_{RF}^t$ [14, 17, 18]. Note that $\mathcal{OB}(m, \mathbb{C})$ is equivalent to the product of m complex circles. Thus, the problem (1) becomes a problem on a complex oblique manifold and a Euclidean space for which systematic procedures are proposed in [19, 20]. Consequently, the problem (1) is conceptually translated into unconstrained optimization problem over the search space $\mathcal{OB}(m, \mathbb{C}) \times \mathbb{R}^{N_{RF}^t \times N_s}$. Hence, ignoring $\|\mathbf{F}_{\mathrm{RF}}\mathbf{F}_{\mathrm{BB}}\|_F^2 = N_s$, the problem (1) is reformulated as

$$\min_{\mathrm{vec}(\mathbf{F}_{\mathrm{RF}}) \in \mathcal{OB}(N_t N_{RF}^t, \mathbb{C})} \; \min_{\mathbf{F}_{\mathrm{BB}} \in \mathbb{R}^{N_{RF}^t \times N_s}} \|\mathbf{F}_{\mathrm{opt}} - \mathbf{F}_{\mathrm{RF}}\mathbf{F}_{\mathrm{BB}}\|_F^2. \tag{3}$$

The inner least-squares optimization problem in (3) is solved in closed form solution $\hat{\mathbf{F}}_{\mathrm{BB}} = \mathbf{F}_{\mathrm{RF}}^{\dagger}\mathbf{F}_{\mathrm{opt}}$ exploiting the least squares structure of the cost function. Hence, the final problem formulation is presented below.

$$\min_{\mathrm{vec}(\mathbf{F}_{\mathrm{RF}}) \in \mathcal{OB}(m, \mathbb{C})} \; \|\mathbf{F}_{\mathrm{opt}} - \mathbf{F}_{\mathrm{RF}}\hat{\mathbf{F}}_{\mathrm{BB}}\|_F^2. \tag{4}$$

Denoting the Euclidean gradient of $\|\mathbf{F}_{\mathrm{opt}} - \mathbf{F}_{\mathrm{RF}}\hat{\mathbf{F}}_{\mathrm{BB}}\|_F^2$ with respect to $\mathbf{F}_{\mathrm{RF}}$ as $\mathbf{G}(\mathbf{F}_{\mathrm{RF}})$, the Euclidean gradient $\nabla f(\boldsymbol{x}) \in \mathbb{R}^{N_t N_{RF}^t}$ of (4) is calculated as

$$\nabla f(\boldsymbol{x}) = \mathrm{vec}(\mathbf{G}(\mathbf{F}_{\mathrm{RF}})) = \mathrm{vec}(-2(\mathbf{F}_{\mathrm{opt}} - \mathbf{F}_{\mathrm{RF}}\hat{\mathbf{F}}_{\mathrm{BB}})\hat{\mathbf{F}}_{\mathrm{BB}}^H). \tag{5}$$

It should be emphasized that this *matrix-based* calculation of $\mathbf{G}(\mathbf{F}_{\mathrm{RF}})$ differs from MO-AltMin, which relies on the vectorization of $\mathbf{F}_{\mathrm{opt}}$ and the Kronecker product of $\mathbf{F}_{\mathrm{BB}}$ as

$$\nabla f(\boldsymbol{x}) = -2(\hat{\mathbf{F}}_{\mathrm{BB}}^* \otimes \mathbf{I}_{N_t})[\mathrm{vec}(\mathbf{F}_{\mathrm{opt}}) - (\hat{\mathbf{F}}_{\mathrm{BB}}^T \otimes \mathbf{I}_{N_t})\boldsymbol{x}]. \tag{6}$$

As a result, this modification drastically reduces the calculation complexity as seen in Section 3.3 and 4.1. Next, the Riemannian gradient at $\boldsymbol{x}$ is obtained by projecting $\nabla f(\boldsymbol{x})$ onto the tangent space $T_{\boldsymbol{x}}\mathcal{OB}(m, \mathbb{C})$ as $\mathrm{grad} f(\boldsymbol{x}) = \mathrm{P}_{\boldsymbol{x}} \nabla f(\boldsymbol{x}) = \nabla f(\boldsymbol{x}) - \mathrm{Real}[\nabla f(\boldsymbol{x}) \circ \boldsymbol{x}^*] \circ \boldsymbol{x}$, where $\mathrm{P}_{\boldsymbol{x}}$ is a projection operator onto $T_{\boldsymbol{x}}\mathcal{OB}(m, \mathbb{C})$ [19]. Finally, the k-th iterate $\boldsymbol{x}^k$ is updated as $\boldsymbol{x}^{k+1} = R_{\boldsymbol{x}^k}(-\alpha^k \xi^k)$, where α^k is a step size, and $\xi^k \in T_{\boldsymbol{x}^k}\mathcal{OB}(m, \mathbb{C})$ is a direction derived from $\mathrm{grad} f(\boldsymbol{x})$. The derivation of ξ^k depends on the algorithm to be used, which is, for example, the Riemannian steepest descent (RSD) and the Riemannian conjugate gradient (RCG) [19, Section 8.3]. $R_{\boldsymbol{x}} : T_{\boldsymbol{x}}\mathcal{M} \to \mathcal{M} : \zeta \mapsto$

Algorithm 1 Proposed algorithm with RSD.

Require: $\mathbf{F}_{\mathrm{opt}}$

1: Initialize $\boldsymbol{x}^0$.
2: **for** $k = 0, 1, 2, \ldots$ **do**
3: Inverse-vectorize $\boldsymbol{x}^k$ as $\mathbf{F}_{\mathrm{RF}}^k = \mathrm{vec}^{-1}(\boldsymbol{x}^k)$.
4: Compute $\hat{\mathbf{F}}_{\mathrm{BB}}^k = (\mathbf{F}_{\mathrm{RF}}^k)^\dagger \mathbf{F}_{\mathrm{opt}}$.
5: Compute the Euclidean gradient $\nabla f(\boldsymbol{x}^k)$ using (5).
6: Compute the Riemannian gradient $\xi^k = \mathrm{P}_{\boldsymbol{x}^k} \nabla f(\boldsymbol{x}^k)$.
7: Find the step size α^k.
8: Update $\boldsymbol{x}^{k+1} = R_{\boldsymbol{x}^k}(-\alpha^k \xi^k)$.
9: **end for**
10: Output $\mathbf{F}_{\mathrm{RF}} = \mathrm{vec}^{-1}(\boldsymbol{x}^{k+1})$ and $\mathbf{F}_{\mathrm{BB}} = \dfrac{\sqrt{N_s}}{\|\mathbf{F}_{\mathrm{RF}} \hat{\mathbf{F}}_{\mathrm{BB}}^k\|_F} \hat{\mathbf{F}}_{\mathrm{BB}}^k$.

$R_{\boldsymbol{x}}(\zeta)$ is called a *retraction* at $\boldsymbol{x}$, and maps tangent space $T_{\boldsymbol{x}}\mathcal{M}$ onto $\mathcal{M}$ with a local rigidity condition that preserves the gradients at $\boldsymbol{x}$. This case uses $R_{\boldsymbol{x}^k}(\alpha^k \xi^k) = [\frac{(\boldsymbol{x}^k + \alpha^k \xi^k)_i}{|(\boldsymbol{x}^k + \alpha^k \xi^k)_i|}]$. After the termination of the loop, $\mathbf{F}_{\mathrm{BB}}$ is obtained by normalizing as $\mathbf{F}_{\mathrm{BB}} = \sqrt{N_s}/\|\mathbf{F}_{\mathrm{RF}} \hat{\mathbf{F}}_{\mathrm{BB}}^k\|_F$ to satisfy the constraint $\|\mathbf{F}_{\mathrm{RF}} \mathbf{F}_{\mathrm{BB}}\|_F^2 = N_s$ in (1).

Now, the extension to OFDM defined in (2) is derived. The Euclidean gradient of $\sum_{l=1}^{L-1} \|\mathbf{F}_{\mathrm{opt}}[l] - \mathbf{F}_{\mathrm{RF}} \hat{\mathbf{F}}_{\mathrm{BB}}[l]\|_F^2$ with respect to $\mathbf{F}_{\mathrm{RF}}$ is calculated instead of (5) as

$$\mathbf{G}(\mathbf{F}_{\mathrm{RF}}) = -2(\mathbf{F}_{\mathrm{opt}}[l] - \mathbf{F}_{\mathrm{RF}} \hat{\mathbf{F}}_{\mathrm{BB}}[l]) \hat{\mathbf{F}}_{\mathrm{BB}}^H[l].$$

Since the following procedure is analogous to that of the narrowband mmWave system, it is omitted.

Lastly, the overall algorithm is summarized in Algorithm 1, where, for simplicity, the RSD is used. It is noteworthy that, comparing with MO-AltMin, the updates of $\hat{\mathbf{F}}_{\mathrm{BB}}$ and $\mathbf{F}_{\mathrm{RF}}$ in the proposed algorithm are mutually integrated into one single-loop structure. This achieves faster convergence of the proposed algorithm.

3.3 Complexity analysis

The proposed algorithm needs to calculate the Euclidean gradient defined in (5), which is the dominant calculation cost of the proposed algorithm. Hence, the computational complexity for the gradient calculation is $\mathcal{O}(N_{RF}^t N_t N_s)$. Meanwhile, the calculation cost of (6) in MO-AltMin algorithm is $\mathcal{O}(N_{RF}^t N_t^3 N_s^2)$ [14]. Apparently, the proposed algorithm has a lower complexity than the MO-AltMin algorithm because the latter relies on the Kronecker product calculation. Thus, as pointed out in [14], the MO-AltMin algorithm is numerically infeasible for large-scale systems in terms of the processing time. Furthermore, since PE-AlgMin requires $\min\{N_s^2 N_{RF}^t, N_s (N_{RF}^t)^2\}$ for the SVD calculation per iteration, the proposed algorithm competes the low-complexity PE-AlgMin algorithm. Consequently, as summarized in Table 1, the proposed algorithm is comparable to or much faster processing than the state-of-the-art algorithms whereas it produces near-optimal spectral efficiency as seen in Section 4.

Table 1: Complexity comparison

Algorithm	Complexity
MO-AltMin [14, Section III]	$\mathcal{O}(N_{RF}^t N_t^3 N_s^2)$
PE-AlgMin [14, Section IV]	$\mathcal{O}(\min\{N_s^2 N_{RF}^t, N_s (N_{RF}^t)^2\})$
Proposed	$\mathcal{O}(N_{RF}^t N_t N_s)$

4 Numerical evaluations

This section evaluates the performance of the proposed algorithm under the same conditions as [14]: The propagation environment is modeled as a $N_{cl} = 8$ cluster environment with $N_{ray} = 10$ rays per cluster with Laplacian distributed azimuth and elevation angles of arrival and departure with uniformly distributed mean angles over $[0, 2\pi)$ and angular spread of 10 degrees [21]. The experiments assume the multi-carrier situation with $L = 128$, and that N_{RF}^t is equal to N_{RF}^r as $N_{RF}^t = N_{RF}^r = N_{RF}$. The RCG algorithm is used for the optimization algorithm. All experiments are executed in MATLAB on a 4.0 GHz Intel Core i7 PC with 32 GB RAM. The codes of the conventional algorithms are downloaded from the authors' site [2].

4.1 Comparison with near-optimal MO-AltMin

This subsection first presents the fast convergence property of the proposed algorithm against MO-AltMin which produces near-optimal spectral efficiency. The parameters are as follows; $N_s = 4$, $N_{RF}^t = N_{RF}^r = 6$ and $(N_t, N_r) = (144, 36)$. Fig.2(a) shows that the spectral efficiency of the proposed algorithm is almost identical to that of MO-AltMin in all SNRs. Fig.2(b) and (c) also show the decrease behaviors of the objective function, i.e., $\|\mathbf{F}_{\text{opt}} - \mathbf{F}_{\text{RF}}\hat{\mathbf{F}}_{\text{BB}}\|_F^2$, with respect to the iteration number and the processing time, respectively. These reveal that the proposed algorithm is much faster than MO-AltMin for both of the metrics. Consequently, the proposed algorithm yields the same spectral efficiency as MO-AltMin with much faster convergence speed than MO-AltMin.

4.2 Spectral efficiency and processing time evaluations

This subsection compares the proposed algorithm with the OMP algorithm [11], the PE-AlgMin algorithm [14, Section IV] and the optimal digital precoder for a benchmark. The MO-AltMin algorithm in [14, Section III] is omit because the spectral efficiency is the same as the proposed algorithm and its processing time is too high to be compared as shown earlier. Fig.3 first presents the spectral efficiency for each SNR in case of $(N_s, N_{RF}^t) = \{(4, 6), (6, 9), (8, 12)\}$ for $(N_t, N_r) = \{(144, 36), (256, 64)\}$. As the figures show, although the PE-AlgMin algorithm gives higher spectral efficiency than the OMP algorithm when $(N_s, N_{RF}^t) = \{(4, 6), (6, 9)\}$, it gives similar values of the OMP algorithm when $(N_s, N_{RF}^t) = (8, 12)$. On the other hand, the proposed algorithm yields stably higher results than both of them, and very close values as the optimal digital precoder.

The performances are next evaluated when changing N_{RF}^t under $N_s = \{6, 8, 12\}$ at $(N_t, N_r) = \{(144, 36), (256, 64)\}$. The range of $N_s < 2N_{RF}^t$ are addressed because $N_s \geq 2N_{RF}^t$ have been thoroughly investigated in [22]. Fig.4(a) and (b) show the spectral efficiency and processing time, respectively. Whereas the spectral efficiency of the PE-AlgMin algorithm is not changed, those of the OMP and proposed algorithm become improved as N_{RF} increases. At the higher range of N_{RF}, the proposed algorithm approaches to the optimal digital precoder at all N_s values. As for the processing

[2] `https://github.com/yuxianghao/`.

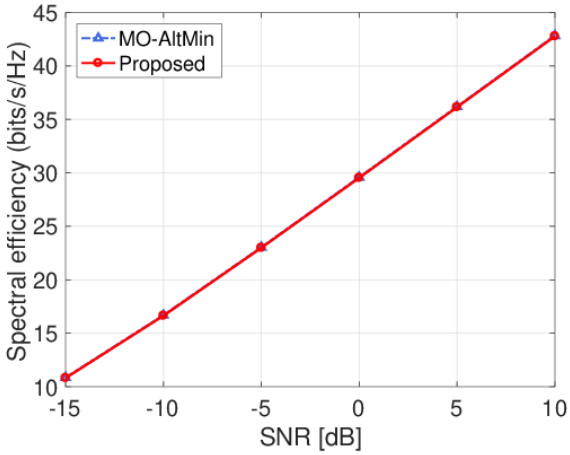

(a) Spectral efficiency

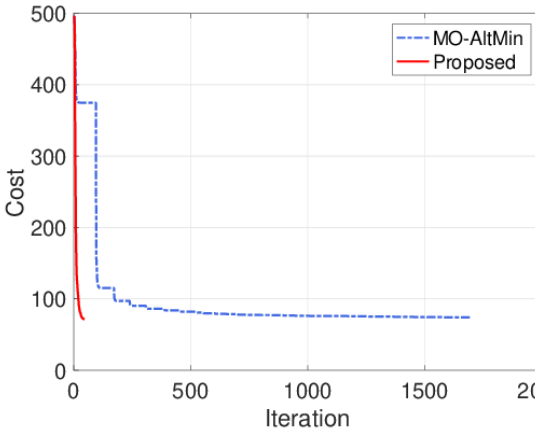

(b) Cost vs. Iteration

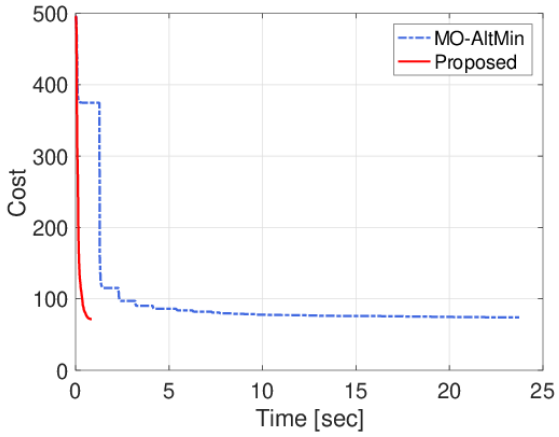

(c) Cost vs. Time [sec]

Figure 2: Spectral efficiency and convergence behaviors.

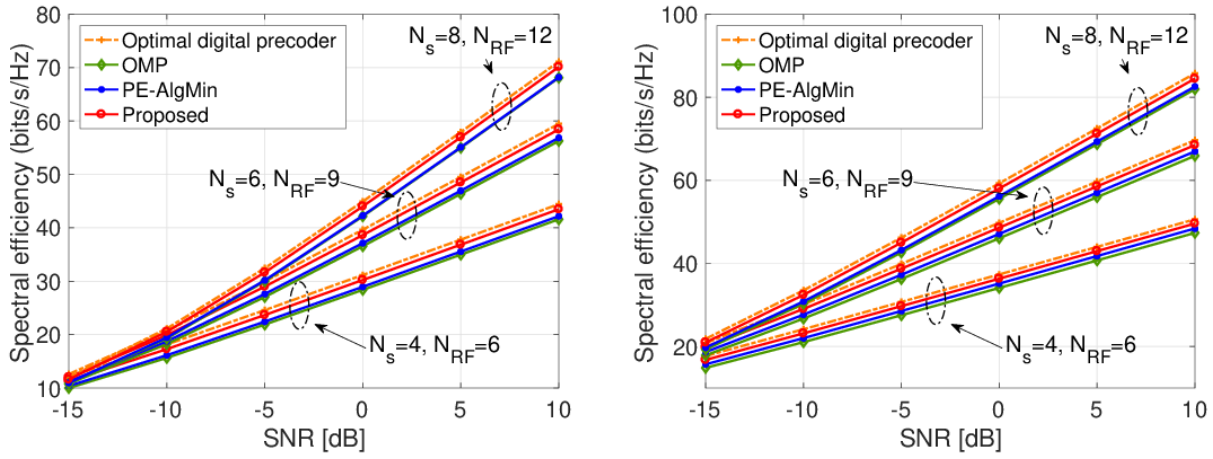

(a) $(N_t, N_r) = (144, 36)$ (b) $(N_t, N_r) = (256, 64)$

Figure 3: Spectral efficiency ($N_s = \{4, 6, 8\}$).

time, the OMP algorithm gives very lower values as expected at the expense of its lower spectral efficiency because it requires only basis searches and no iterations for optimization. Meanwhile, although the PE-AlgMin algorithm gives lower processing time than the propose algorithm for $N_s = 6$, it is hindered by the higher processing time than the proposed algorithm when higher N_{RF} and N_s. These results are coincident with Table 1 in terms of the sizes and orders of N_s and N_{RF}. To conclude, the proposed algorithm achieves near-optimal spectral efficiency with a comparable to or lower processing complexity than PE-AlgMin for a large-scale system with higher N_s and N_{RF}.

5 Conclusions

This paper has proposed a fast optimization algorithm for a hybrid precoder design in millimeter wave systems. The numerical experiments demonstrated the superior performance of the proposed algorithm in terms of the comparable to or higher spectral efficiency than the state-of-the-art algorithms including MO-AltMin algorithm, and comparable or faster processing than the low-complexity PE-AltMin algorithm.

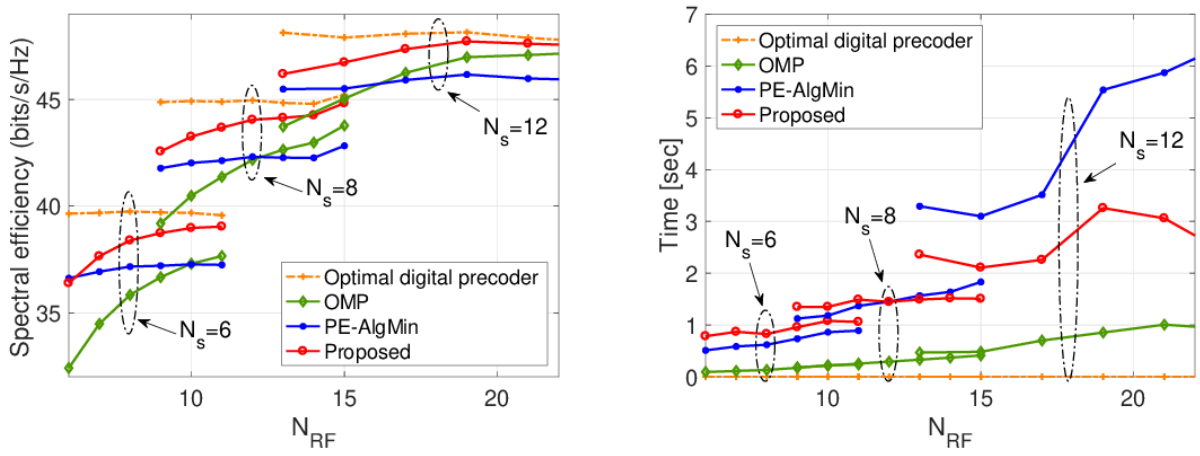

(a) $(N_t, N_r) = (144, 36)$

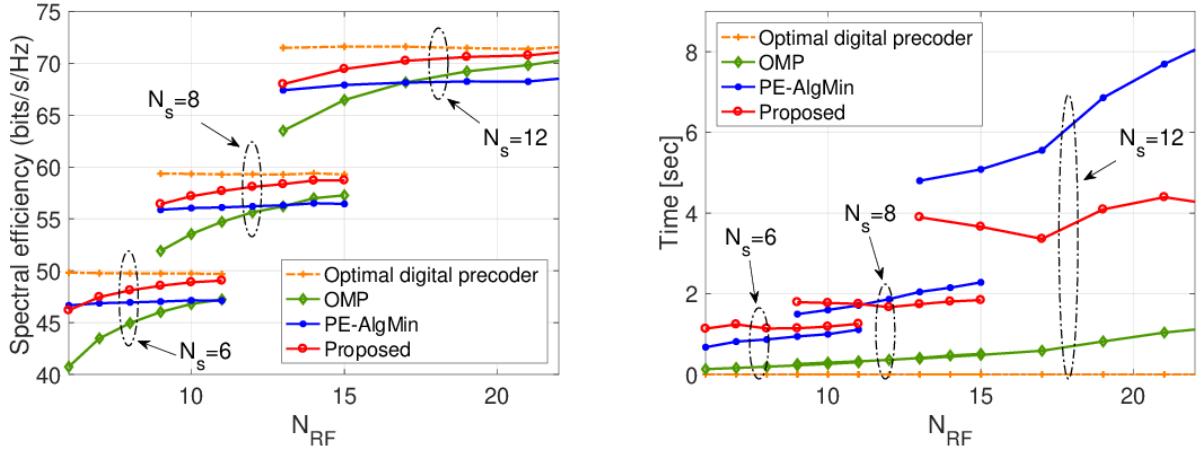

(b) $(N_t, N_r) = (256, 64)$

Figure 4: Spectral efficiency and processing time.

References

[1] S. Khiong and C.-C. Chong. An overview of multigigabit wireless through millimeter wave technology: Potentials and technical challenges. *EURASIP Journal on Wireless Communications and Networking*, 2007(1), 2006.

[2] R. W. Daniels, R. C. Heath. 60 GHz wireless communications: Emerging requirements and design recommendations. *IEEE Vehicular Technology Magazine*, 2(3):41–50, 2007.

[3] C.H. Doan, S. Emami, D.A. Sobel, A.M. Niknejad, and R.W. Brodersen. Design considerations for 60 GHz CMOS radios. *IEEE Communications Magazine*, 42(12):132–140, 2004.

[4] T. S. Rappaport, R. W. Heath Jr., R. C. Daniels, and J. N. Murdock. *Millimeter Wave Wireless Communications*. Prentice Hall, 2014.

[5] M. R. Akdeniz, Y. Liu, M. K. Samimi, S. Sun, S. Rangan, T. S. Rappaport, and E. Erkip. Millimeter wave channel modeling and cellular capacity evaluation. *IEEE Journal on Selected Areas in Communications*, 32(6):1164–1179, 2014.

[6] H. Seleem, A. S. Sulyman, and A. Alsanie. Hybrid precoding-beamforming design with hadamard RF codebook for mmWave large-scale MIMO systems. *IEEE Access*, 5:6813–6823, 2017.

[7] Z. Pi and F. Khan. An introduction to millimeter-wave mobile broadband systems. *IEEE Communications Magazine*, 49(6):101–107, 2011.

[8] F. Rusek, D. Persson, B. K. Lau, E. G. Larsson, T. L. Marzetta, O. Edfors, and F. Tufvesson. Scaling up MIMO: Opportunities and challenges with very large arrays. *IEEE Signal Processing Magazine*, 30(1):40–60, 2013.

[9] X. Zhang, A. F. Molisch, and S.-Y. Kung. Variable-phase-shift-based RF-baseband codesign for MIMO antenna selection. *IEEE Transactions on Signal Processing*, 53(11):4091–4103, 2005.

[10] V. Venkateswaran and Veen A.-J. v. d. Analog beamforming in MIMO communications with phase shift networks and online channel estimation. *IEEE Transactions on Signal Processing*, 58(8):4131–4143, 2010.

[11] O. E. Ayach, S. Rajagopal, S. Abu-Surra, Z. Pi, and R. W. Heath. Spatially sparse precoding in millimeter wave MIMO systems. *IEEE Transations on Wireless Communications*, 13(3):1499–1513, 2014.

[12] A. Alkhateeb, O. E. Ayach, G. Leus, and R. W. Heath. Channel estimation and hybrid precoding for millimeter wave cellular systems. *IEEE Journal of Selected Topics in Signal Processing*, 8(5):831–846, 2014.

[13] Y. Lee, C.-H. Wang, and Y.-H. Huang. A hybrid RF/baseband precoding processor based on parallel-index-selection matrix-inversion-bypass simultaneous orthogonal matching pursuit for millimeter wave MIMO systems. *IEEE Transactions on Signal Processing*, 63(2):305–317, 2015.

[14] X. Yu, J.-C. Shen, J. Zhang, and K. B. Letaief. Alternating minimization algorithms for hybrid precoding in millimeter wave MIMO systems. *IEEE Journal on Selected Areas in Communications*, 10(3):485–500, 2016.

[15] N. B. Zanjani, S. Khademi, and G. Leus. Gradient-based solution for hybrid precoding in MIMO systems. In *IEEE International Conference on Acoustics, Speech and Signal Processing (ICASSP)*, 2017.

[16] N. Boumal, B. Mishra, P.-A. Absil, and R. Sepulchre. Manopt: a Matlab toolbox for optimization on manifolds. *JMLR*, 15(1):1455–1459, 2014.

[17] P.-A. Absil and K. A. Gallivan. Joint diagonalization on the oblique manifold for independent component analysis. In *IEEE International Conference on Acoustics Speech and Signal Processing Proceedings (ICASSP)*, 2006.

[18] H. Shen and M. Kleinsteuber. A matrix joint diagonalization approach for complex independent vector analysis. In F. Theis, A. Cichocki, A. Yeredor, and M. Zibulevsky, editors, *Latent Variable Analysis and Signal Separation. LVA/ICA 2012*, Lecture Notes in Computer Science, pages 66–73. Springer, 2012.

[19] P.-A. Absil, R. Mahony, and R. Sepulchre. *Optimization Algorithms on Matrix Manifolds*. Princeton University Press, 2008.

[20] A. Edelman, T.A. Arias, and S.T. Smith. The geometry of algorithms with orthogonality constraints. *SIAM J. Matrix Anal. Appl.*, 20(2):303–353, 1998.

[21] H. Xu, V. Kukshya, and T. S. Rappaport. Spatial and temporal characteristics of 60-GHz indoor channels. *IEEE Journal on Selected Areas in Communications*, 20(3):620–630, 2001.

[22] E. Zhang and C. Huang. On achieving optimal rate of digital precoder by RF-baseband codesign for MIMO systems. In *IEEE 80th Vehicular Technology Conference (VTC2014-Fall)*, 2014.